Entropy and Volume Change of Dissociation in Tobacco Mosaic Virus Probed by High Pressure

ARTICLE *in* THE JOURNAL OF PHYSICAL CHEMISTRY B · DECEMBER 2012

Impact Factor: 3.3 · DOI: 10.1021/jp310219k · Source: PubMed

6 AUTHORS, INCLUDING:

Carlos F S Bonafe
University of Campinas
25 PUBLICATIONS **299** CITATIONS
SEE PROFILE

Ernesto Acosta Martínez
Universidade Estadual de Feira de Santana
21 PUBLICATIONS **72** CITATIONS
SEE PROFILE

Douglas R. Norberto
Institut Pasteur
9 PUBLICATIONS **154** CITATIONS
SEE PROFILE

THE JOURNAL OF PHYSICAL CHEMISTRY B

Article

pubs.acs.org/JPCB

Entropy and Volume Change of Dissociation in Tobacco Mosaic Virus Probed by High Pressure

Jose A. C. Bispo,*[,†] Carlos F. S. Bonafe,[‡] Ines Joekes,[§] Ernesto A. Martinez,[†] Giovani B. M. Carvalho,[†] and Douglas R. Norberto[‡]

[†]Departamento de Tecnologia (DTEC), Curso de Engenharia de Alimentos, Universidade Estadual de Feira de Santana (UEFS), CP 252/294, Feira de Santana, BA, CEP 44036-900, Brazil

[‡]Laboratório de Termodinâmica de Proteínas, Departamento de Bioquímica, Instituto de Biologia, Campinas, SP, CEP 13083-970, Brazil

[§]Departamento de Físico Química, Instituto de Química, Universidade Estadual de Campinas (UNICAMP), Campinas, SP, CEP 13083-970, Brazil

ABSTRACT: Virus dissociation and inactivation by high pressure have been extensively studied in recent decades. Pressure-induced dissociation of viral particles involves a reduction in the Gibbs free energy of dissociation and a negative change in volume. In this work, we investigated the combined effect of high pressure and temperature on the dissociation of tobacco mosaic virus (TMV). We assumed the presence of two states of TMV with different tendencies to dissociate. Thus one form presents a low tendency (L) and the other a high tendency (H) to dissociate. Based on the model described here, the L−H transition was favored by an increase in pressure and a decrease in temperature. The volume change of dissociation was pressure- and temperature-dependent, with a highly negative value of −80 mL/mol being recorded at 0 °C and atmospheric pressure. The entropy and enthalpy of dissociation were very temperature- and pressure-dependent, with values of entropy of 450 to −1300 kJ/mol and values of enthalpy of 5.5×10^4 to 2.4×10^4 kJ/mol. The dissociation of TMV was enthalpy-driven at all temperatures and pressures investigated. Based on these findings, we conclude that the model presented allows accurate predictions of viral dissociation behavior in different experimental conditions.

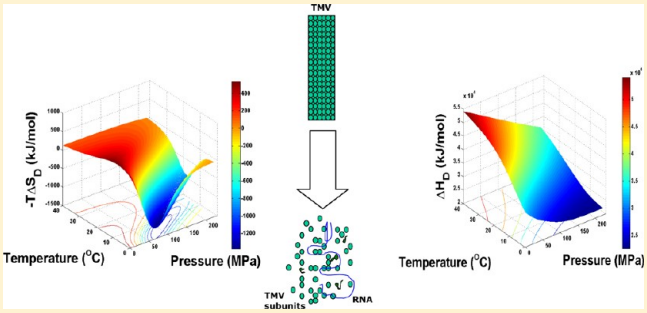

INTRODUCTION

Subunit assembly in high protein aggregates has been studied using several approaches in different biological models. Our understanding of these processes has gradually expanded through the careful control of variables such as temperature, pH, ionic strength, and pressure. In particular, the use of high-pressure incubations (up to 300 MPa) has provided important information about the mechanisms of aggregation since pressure produces no significant alterations in the tertiary structure of proteins.[1−3] The latter characteristic is important when using high pressure to develop experimental vaccines because viral inactivation without significant structural changes in the viral capsid helps to maintain immunogenic properties.[4−7] Virus inactivation by pressure has also been studied as a means of sterilization,[5,8,9] and pressure has been used to investigate the thermodynamics of virus dissociation.[5,7,10−13] Enveloped viruses, which have a lipid membrane in their structure, are also targets of pressure-induced inactivation.[14,15] The combined effect of high pressure and other factors, such as subzero temperatures, different conditions of pH, and the presence of subdenaturant concentrations of urea, has provided insights into the protein−protein interactions that drive aggregation, with the advantage that such methods avoid the need to use extreme temperatures to promote protein dissociation.[2] This approach has been used to study urea-mediated denaturation in well-defined conditions.[16,17]

Accurate knowledge of the properties of virus aggregation is crucial for understanding virion stability and the dissociation that occurs during infection. Tobacco mosaic virus (TMV) is a rod-shaped virus with 2130 subunits of 17.5 kDa protecting a 6.4 kb molecule of single positive RNA strand. The physiopathology of the disease elicited by TMV in the host plant is related to the biophysical properties of the TMV coat protein.[18] The virus−host cell interaction is fundamental for the pathogenesis of infection, and several important proteins participate in this process.[18,19] Extensive studies of the structural and aggregation properties of TMV particles have led to this virus becoming a textbook model of biological assembly.[20,21] Interestingly, the first transgenic virus-resistant plants were tobacco plants that expressed the TMV coat protein,[22] which effectively resulted in inhibition of the uncoating of the virus particles.[23]

Received: October 16, 2012
Revised: November 30, 2012
Published: December 3, 2012

TMV undergoes dissociation at high pressure that is much more efficient at low temperature (≤0 °C).[24] A combination of high pressure and alkaline conditions[25] and the presence of urea[17] also promote dissociation. The dissociation of viral coat protein at high pressure is markedly enhanced by the absence of viral RNA, indicating an important role for viral RNA in stabilizing the aggregate.[24] Some native high-protein aggregates with no associated nucleic acid, such as annelid extracellular hemoglobin[26,27] and hemocyanin,[28] show a similar dissociation profile to that observed for TMV coat protein.

Although the effect of temperature on the stability of coat protein preparations has been investigated,[29,30] little is known of the thermal dependence of this process and its physiological implications. The aim of this work was to investigate the influence of pressure and temperature on the thermodynamics of TMV dissociation. For this analysis, we assumed the presence of two states of TMV with different tendencies to dissociate. This assumption allowed an efficient description of dissociation as well as highly accurate predictions of dissociation under different combinations of pressure and temperature. Overall, the model provided accurate thermodynamic information on the entropy and volume dependence of dissociation. Although TMV is not normally exposed to the level of pressure and extreme temperatures used here, and the host cell concentration of TMV is much lower than that tested in this work (in addition to the presence of numerous intracellular factors that can elicit viral disassembly), investigations such as that described here are important for evaluating the energy involved in the dissociation process and for furthering our understanding of the virion state in the host cell. The presented approach can be used to examine the influence of a variety of conditions on virus properties and may be useful in improving biotechnological processes.

MATERIALS AND METHODS

Chemicals. All reagents were of analytical grade. Distilled water was filtered and deionized through a Millipore water purification system (18 MΩ resistance). All experiments were done in quadruplicate, in 50 mM Tris-HCl, pH 8.0, and for each experimental temperature the pH of the buffer was always checked and adjusted to 8.0 when necessary. The TMV concentration was 0.5 mg/mL.

TMV Purification. TMV was isolated from Turkish tobacco plants infected with the common strain of the virus. The virus was purified as described by Asselin and Zaitlin.[31] Briefly, frozen (−70 °C) infected leaves were homogenized in a Waring blender, filtered, and mixed with Celite for clarification. The supernatant was combined with PEG 6000 and NaCl, precipitated at 0 °C, centrifuged, and resuspended in 0.01 M Na_2HPO_4 and 0.01% (w/v) Na-ascorbate. The Celite/PEG treatment was repeated, and the resuspension was combined with Triton X-100 and ultracentrifuged. The pellet was resuspended in 1 mM EDTA, pH 7.2, and centrifuged for clarification. The supernatant was stored at 4 °C.

Light Scattering and Fluorescence under Pressure. The high-pressure system used here has been described elsewhere.[32] An ISS model HP high-pressure cell with sapphire windows connected to a pressure generator (HIP) was used. The light scattering at 340 nm was monitored in an Edinburgh FL900 spectrofluorimeter at an angle of 90° relative to the incident light using the same wavelength for the excitation and emission monochromators. Since there is a linear correlation between light scattering intensity and virus concentrations up to 1.0 mg of TMV/mL,[25] the average molecular weight was estimated based on the intensity of light scattering (eqs 17−32 in Tanford[33]) at pressure P (I_P). The average degree of dissociation was considered to be proportional to the average molecular weight in solution. We assumed that the viral solution had a degree of dissociation zero at atmospheric pressure and 40 °C, and 1 for the light scattering intensity equal to the buffer solution only. The average degree of dissociation at pressure P was calculated by using the relationship

$$\hat{\alpha}(P) = \frac{I_i - I_P}{I_i - I_f} \tag{1}$$

where I_i and I_f are the intensities of light scattering corresponding to the associated and dissociated forms, respectively. TMV was subjected to temperatures ranging from 0 to 40 °C. This range is very convenient since TMV undergoes nearly 100% dissociation at 250 MPa and 0 °C,[24] as also confirmed here. The temperature in the pressure cell was measured directly with a temperature probe and controlled by a thermostat-regulated circulating water bath (Marconi, MA-184). The temperature of the pressure cell was unaffected by the changes in pressure.

TMV solutions (0.5 mg/mL in Tris-HCl, pH 8.0) were preincubated for 2 h at the desired temperature to allow equilibration of the solution. The samples were subsequently incubated for 15 min at each pressure value prior to the light scattering measurement, which typically lasted 1 min.

Thermodynamic Approach. We assumed the presence of two forms of virus in solution, one with a low tendency to dissociate and the other with a high tendency to dissociate (based on strong and weak protein−protein interactions, respectively). The corresponding degrees of dissociation were designated by the subscript L for the species with a low tendency to dissociate and H for the species with a high tendency to dissociate. The following equilibrium relationships were assumed

$$P_{n\mathrm{L}} \overset{K_\mathrm{L}}{\rightleftarrows} nP_\mathrm{L}$$

$$P_{n\mathrm{H}} \overset{K_\mathrm{H}}{\rightleftarrows} nP_\mathrm{H}$$

where n is the number of subunits, $P_{n\mathrm{L}}$ and $P_{n\mathrm{H}}$ correspond, respectively, to the viral particles with low and high tendencies to dissociate, and P represents the individual subunits in the L and H states. The pressure dependence of the viral particle in each state is given by the following exponential equation that defines the molar compressibility coefficient (k):

$$k = -\frac{1}{[P_n]}\left(\frac{\mathrm{d}[P_n]}{\mathrm{d}P}\right)_T \tag{2}$$

In an analogous manner, the concentration dependence of each species with respect to pressure was also analyzed in relation to temperature by using the molar thermal expansibility coefficient, $\theta_\mathrm{M} = 1/[P_n](\mathrm{d}[P_n]/\mathrm{d}T)_P$. The integration of $[P_n](P)$ in eq 2 with respect to pressure P using the boundary conditions of $[P_n](0) = \exp(w)$ furnished the following relationships for the species L and H

$$[P_n]_\mathrm{L}(P) = [P_n]_\mathrm{L}(0)\exp(-k_\mathrm{L}P) = \exp(w_\mathrm{L} - k_\mathrm{L}P) \tag{3}$$

$$[P_n]_\mathrm{H}(P) = [P_n]_\mathrm{H}(0)\exp(-k_\mathrm{H}P) = \exp(w_\mathrm{H} - k_\mathrm{H}P) \tag{4}$$

where w and k are parameters that coordinate the concentration dependence of the viral particle at each pressure. Note that parameter w was correlated to the natural logarithmic of the initial virus concentration, while parameter k reflected the relationship between the associated virus concentration and pressure. In this context, the average degree of dissociation $\hat{\alpha}$ was assumed to be modulated by the concentration of species $[P_n]_L$ and $[P_n]_H$ such that the proportion of these associated species will be given by

$$f_L(P) = \frac{[P_n]_L(P)}{[P_n]_L(P) + [P_n]_H(P)} \tag{5}$$

and

$$f_H(P) = \frac{[P_n]_H(P)}{[P_n]_L(P) + [P_n]_H(P)} \tag{6}$$

Equations 3 and 4 can then be introduced into eqs 5 and 6 to give

$$f_L(P) = \frac{\exp(w_L - k_L P)}{\exp(w_L - k_L P) + \exp(w_H - k_H P)} \tag{7}$$

$$f_H(P) = \frac{\exp(w_H - k_H P)}{\exp(w_L - k_L P) + \exp(w_H - k_H P)} \tag{8}$$

The average degree of viral particle dissociation at pressure P, $\hat{\alpha}(P)$, can therefore be expressed as a function of these species as

$$\hat{\alpha}(P) = f_L(P)\alpha_L + f_H(P)\alpha_H \tag{9}$$

where α_L and α_H are the degrees of dissociation of species L and H. From eqs 7 and 8, it follows that

$$\hat{\alpha}(P) = \frac{\exp(w_L - k_L P)}{\exp(w_L - k_L P) + \exp(w_H - k_H P)}\alpha_L + \frac{\exp(w_H - k_H P)}{\exp(w_L - k_L P) + \exp(w_H - k_H P)}\alpha_H \tag{10}$$

Equation 10 can then be used to fit the experimental data for the degree of dissociation to obtain the six unknown parameters at each temperature condition (w_L, k_L, w_H, k_H, α_L, and α_H). This equation can be simplified to four parameters (w_1, k_1, α_L, and α_H) by dividing the numerator and denominator by $\exp(w_H - k_H P)$, which gives

$$\hat{\alpha}(P) = \frac{\exp(w_1 + k_1 P)}{1 + \exp(w_1 + k_1 P)}\alpha_L + \frac{1}{1 + \exp(w_1 + k_1 P)}\alpha_H \tag{11}$$

where $w_1 = w_L - w_H$ and $k_1 = -k_L + k_H$, from which it follows that

$$f_L(P) = \frac{\exp(w_1 + k_1 P)}{1 + \exp(w_1 + k_1 P)} \tag{12}$$

and

$$f_H(P) = \frac{1}{1 + \exp(w_1 + k_1 P)} \tag{13}$$

Examination of eqs 11−13 indicates that the values of these parameters can be obtained by a nonlinear fit of the experimental data for $\hat{\alpha}(P)$ versus P at each temperature. Although the values for w_1, k_1, α_L, and α_H will be constant with respect to pressure, they will be temperature-dependent, leading to the need for a second adjustment of these parameters to obtain a theoretical description of the results with respect to temperature and the surface plots (Figure 2 below). In these cases, an equation analogous to eq 11 can be used, but now rewritten for temperature dependence in terms of θ_M. With this approach, the model can fit any theoretical conditions of pressure and temperature, thereby allowing precise predictions of the dissociation process.

From eqs 11−13 it is also possible to obtain all of the parameters involved in the dissociation, including species concentration, Gibbs free energy of dissociation, changes in volume, entropy, and enthalpy, and others. For this, we start from the following assumptions

$$[P_n] = (1 - \hat{\alpha}(P))C_{P_n} \tag{14}$$

where C_{P_n} is the initial TMV concentration, and

$$[P] = n\hat{\alpha}(P)C_{P_n} \tag{15}$$

Since the fractions $f_L(P)$ and $f_H(P)$ represent the amount of viral particle species at each pressure and temperature in states L and H ($[P_n]_L$ and $([P_n]_H$) respectively, it follows that

$$[P_n]_L = f_L(P)[P_n] \tag{16}$$

and

$$[P_n]_H = f_H(P)[P_n] \tag{17}$$

From eqs 14 and 15, we also find that

$$K_D = \frac{[P]^n}{[P_n]} \tag{18}$$

and

$$\Delta G_D = -RT \ln\left(\frac{[P]^n}{[P_n]}\right) \tag{19}$$

From these relationships, it follows that

$$\Delta G_{LH} = -RT \ln\left(\frac{[P_n]_H}{[P_n]_L}\right) = -RT \ln\left(\frac{f_H(P)}{f_L(P)}\right) \tag{20}$$

where K_D and ΔG_D are, respectively, the dissociation constant and the Gibbs free energy of dissociation. R corresponds to the gas constant, and ΔG_{LH} is the Gibbs free energy change for the transition of species L to species H.

Differentiation of eq 19 with respect to pressure and temperature (based on Maxwell thermodynamic relationships) yields

$$V_D = \left(\frac{d\Delta G_D}{dP}\right)_T \tag{21}$$

and

$$S_D = -\left(\frac{d\Delta G_D}{dT}\right)_P \tag{22}$$

which gives

$$\Delta H_D = \Delta G_D + T\Delta S_D \tag{23}$$

Consequently, eqs 11−23 allow complete analysis of dissociation in this system under the specified conditions and provide important parameters for understanding and predicting

dx.doi.org/10.1021/jp310219k | J. Phys. Chem. B 2012, 116, 14817−14828

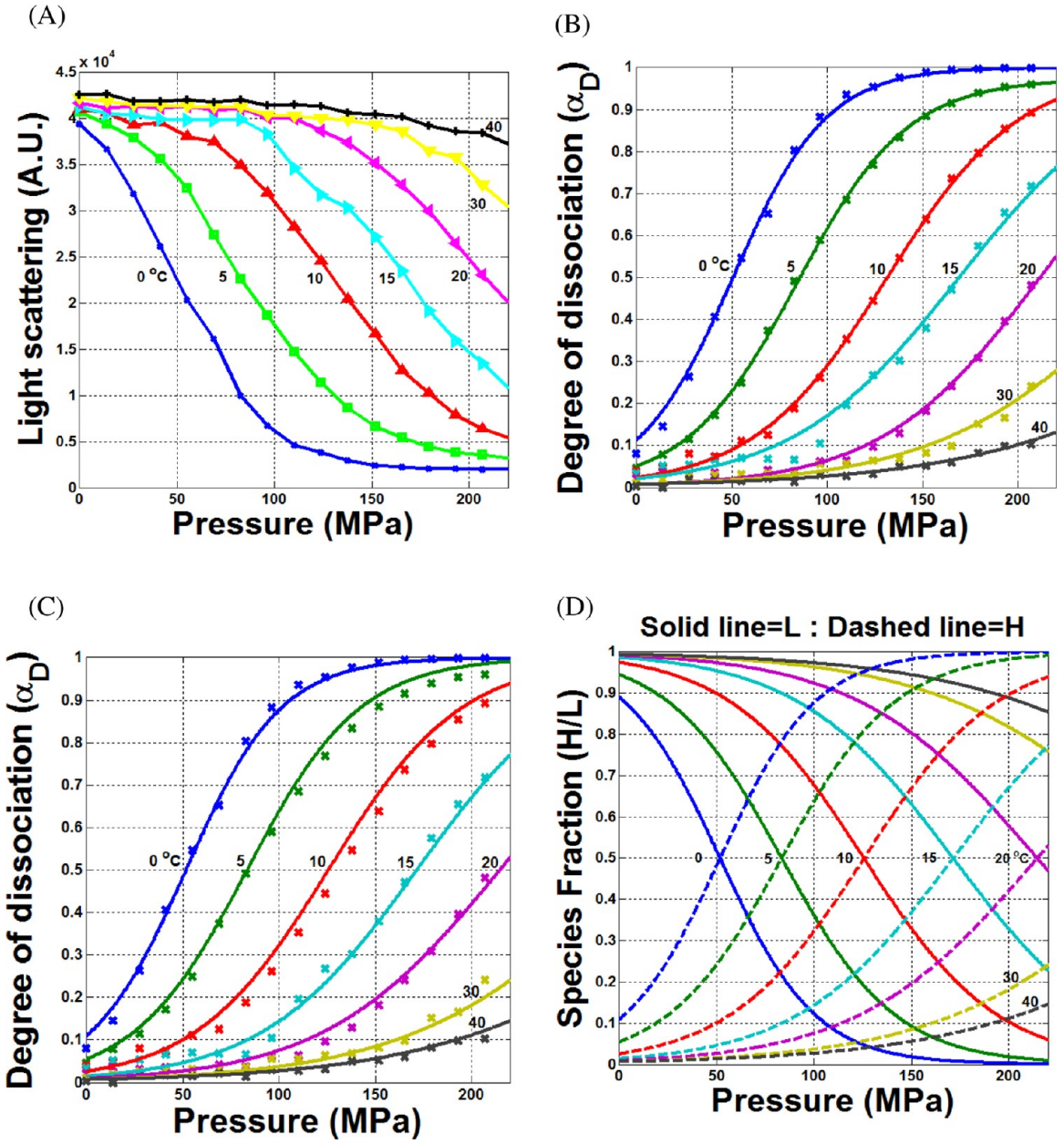

Figure 1. (A) Intensity of light scattering by TMV at different temperatures as a function of pressure. (B) Degree of TMV dissociation αD ($\equiv\hat{\alpha}$) based on light scattering. The data points are from Figure 1A, and the lines were calculated using eq 1. (C) Surface results obtained from surface cuts at the same temperatures, from the fitting procedure described by eq 11 and Figure 2. (D) Fraction of theoretical species in the low-affinity (dashed lines) and high-affinity (continuous line) states at the same temperatures, where f_L and f_H are given by eqs 12 and 13, respectively, and by Figure 2. The experiments were done in quadruplicate. The standard deviations are smaller than the symbols used.

viral dissociation, disaggregation, and denaturation. For the description of more complex heterogeneous systems, eq 9 can be generalized by introducing more states of affinity. In this context, and considering n distinct structures, it follows that

$$\hat{\alpha}(u) = \sum_{i=1}^{n} f_i(u)\alpha_i \tag{24}$$

where f_i corresponds to the fraction of structure species i in solution so that the intrinsic property α_i represents the average degree of dissociation of the ith structure assumed and u is the independent variable of the average function $\hat{\alpha}$. Thus, for a three-structure transition (n = 3), eq 24 reduces to $\hat{\alpha}(u) = f_1(u)\alpha_1 + f_2(u)\alpha_2 + f_3(u)\alpha_3$.

The independent variable u may represent the time t, the effector concentration, or some other parameter such that the species concentration dependence with respect to these properties furnishes functions analogous to those described by eqs 3 and 4. This can be shown by using the rate equation and the concept of extent of reaction, as previously described[34,35] for enzyme systems, for an irreversible process

$$P_n \xrightarrow{k_u} nP \tag{25}$$

where k_u corresponds to the rate constant of virus dissociation with the property u.

The solution for this situation with respect to the species concentration and the initial virus concentration c implies that

dx.doi.org/10.1021/jp310219k | J. Phys. Chem. B 2012, 116, 14817−14828

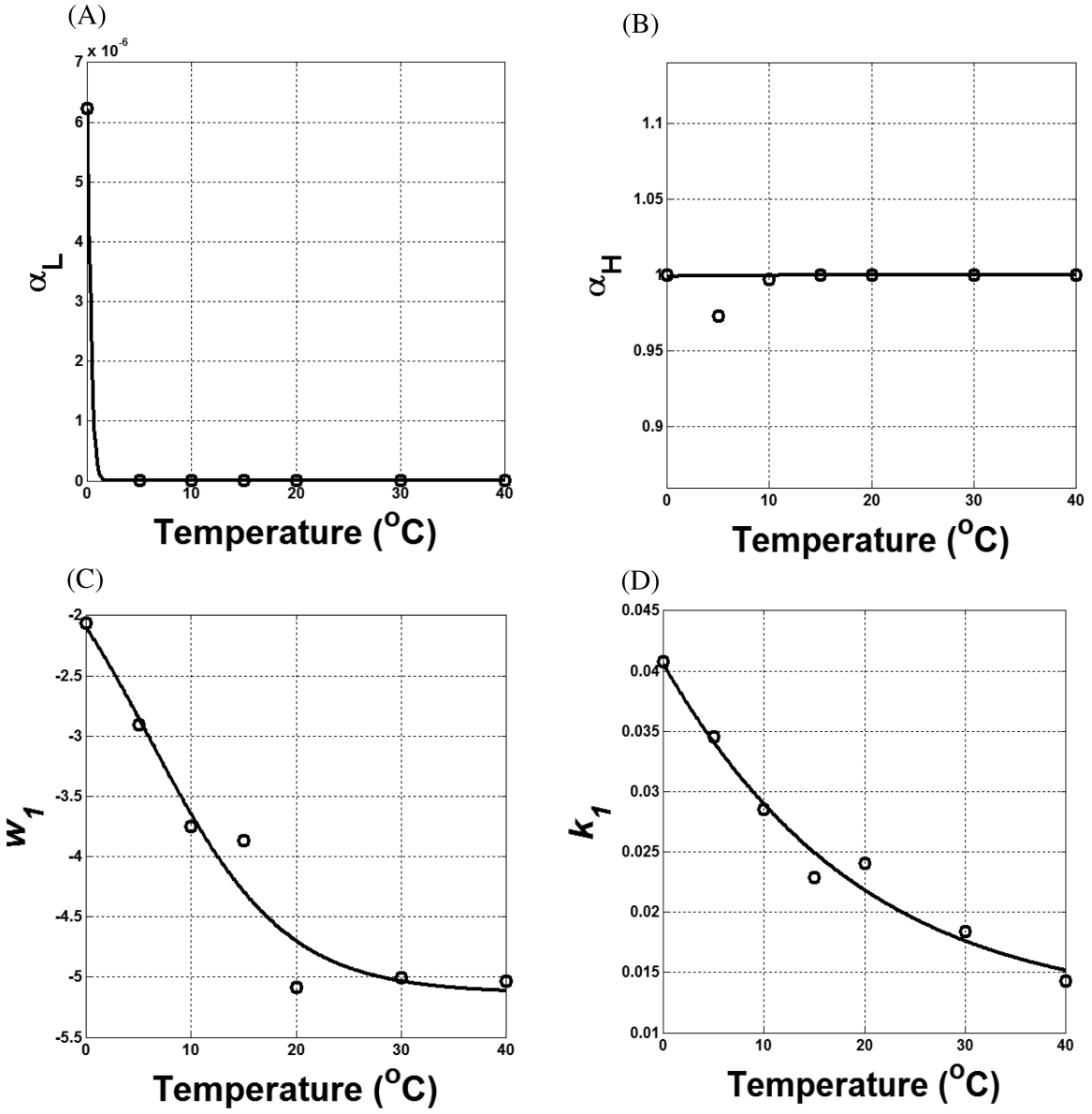

Figure 2. Curve fitting for the experimental results shown in Figure 1B. Equation 11 was used to obtain the parameters α_1 (A), α_2 (B), w_1 (C), and k_1 (D) at each temperature. The respective function for each parameter based on eq 11 is represented by the lines. The standard deviations are smaller than the symbols used.

this system should be described as previously done in terms of the extent of reaction x and the velocity of reaction v,[34,35] as follows

$$[P_n](u) = c - x(u) \tag{26}$$

and

$$v(u) = \frac{dx(u)}{du} = k_u(c - x(u)) \tag{27}$$

Integration of eq 27 furnishes

$$x(u) = c(1 - \exp(-k_u u)) \tag{28}$$

Finally, introducing eq 28 into eq 26 gives

$$[P_n](u) = c\cdot\exp(-k_u u) \tag{29}$$

For $u = P$ and $c = [P_n](0)$, eq 29 becomes analogous to eqs 3 and 4, as well as for other properties such as time, ionic strength, pH effect, and other variables. Inspection of this equation also suggests that it could be used to describe several biotechnological processes such as drying (Newton equation),[36] as well as physical and chemical kinetics that involve decay, volume changes, ligand binding by proteins, protein aggregation, and others.

RESULTS AND DISCUSSION

The effect of temperature and pressure on the state of TMV aggregation was evaluated based on the light scattering profile. As shown in Figure 1A, there was a decrease in light scattering as the pressure increased, indicating dissociation; this process was markedly enhanced by lowering the temperature. As expected, the volume change between the viral particle and its subunits was negative such that the Gibbs free energy of dissociation decreased with increasing pressure and the dissociation was exothermic over the temperature range studied. This tendency to dissociate under pressure and at low temperatures has been observed in other studies that used

dx.doi.org/10.1021/jp310219k | J. Phys. Chem. B 2012, 116, 14817−14828

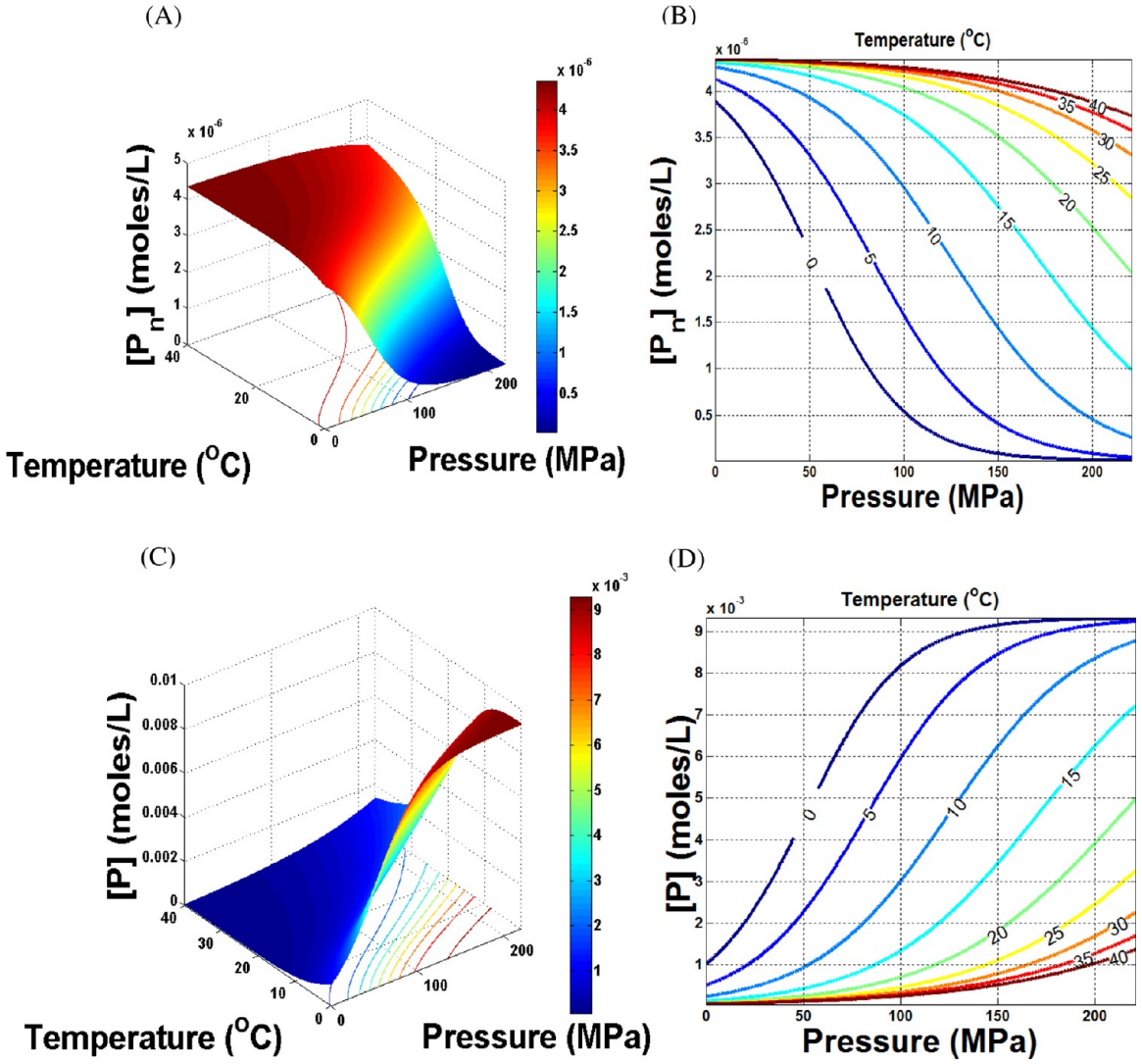

Figure 3. Surface plots of the temperature and pressure dependence of (A) the virus particle concentration, $[P_n]$, according to eq 14, and (C) the virus subunit concentration, $[P]$, according to eq 15. (B) and (D) show the respective contour plots at distinct temperatures.

light scattering, gel filtration, and electron microscopy.[24] Other conditions, such as an increase in pH[25] and the presence of subdenaturing concentrations of urea,[17] can also facilitate the pressure-induced dissociation of TMV. Figure 1B shows the adjustment of eq 11 to the experimental data for the degree of dissociation in which eq 1 was used to convert light scattering to degree of dissociation. There was strong agreement between the fitting function (lines) and the experimental results (symbols), with the coefficient of determination (R^2) reaching values of 0.94 and 0.99 in most cases. The fitting functions were applied to each temperature, and the respective values for α_L, α_H, w_1, and k_1 are shown in Figure 2A–D (symbols). Nonlinear fitting of these values was done using eq 11 rewritten for the temperature dependence of this process, and the results are shown as solid lines in Figure 2A–D. As shown in Figure 2A and B, the results yielded α_L close to 0 and α_H close to 1. In this figure, the experimental symbols and adjustment functions were defined better with respect to the changes in temperature and should allow the prompt analysis of cases not studied in this work. The accuracy of these processes depends on the precision of the fitting functions. Figure 1C shows the final adjustment of the theoretical functions provided by these fitting functions in relation to the experimental data. As can be seen, the two stages of curve fitting provided a theoretical surface with level diagrams (lines) that did not deviate significantly from the theoretical and experimental results. The results obtained from curve fitting in this figure were more reliable than the simple adjustment shown in Figure 1B since they were based on all of the data collected at different temperatures.

The parameters determined from the fitted curves in Figure 2, i.e., α_L, α_H, w_1 and k_1 from eq 11, were used to determine the pressure and temperature dependence of species L and H according to eqs 12 and 13, respectively, for the pressure and temperature ranges analyzed (Figure 1D). This figure shows that initially, at low pressure, the species with a low tendency to dissociate (L) predominated in solution and that its concentration decreased with increasing pressure at all temperatures studied (solid lines in this panel). The fraction of species H increased symmetrically with the decrease in f_L (dashed line in this figure). For each 10 °C rise in temperature, there was a curve shift corresponding to 75 MPa.

The parameters α_L, α_H, w_1, and k_1 obtained from Figure 2 showed good agreement with the experimental data and were used for a more complete thermodynamic description of the

dx.doi.org/10.1021/jp310219k | J. Phys. Chem. B 2012, 116, 14817–14828

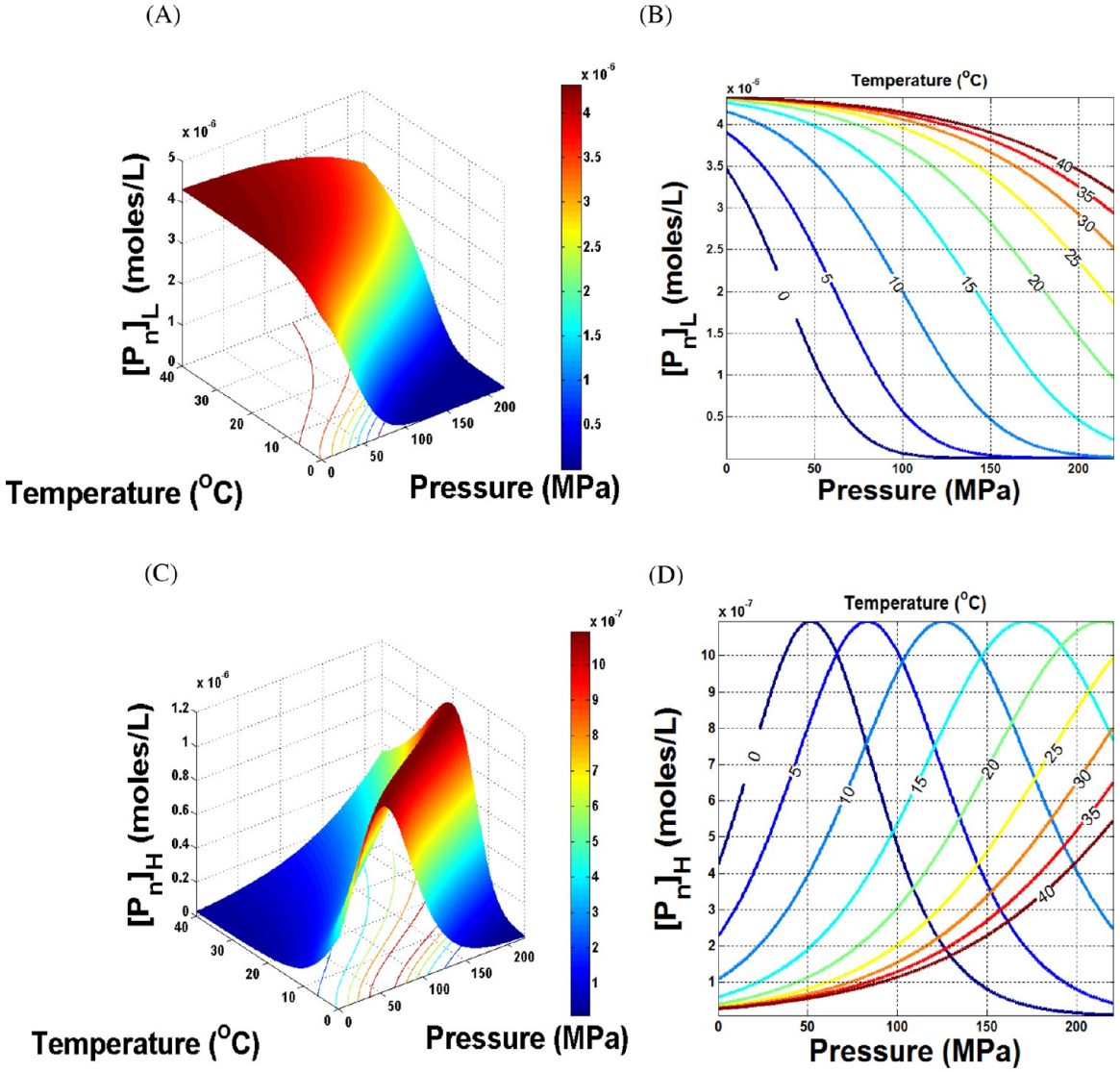

Figure 4. Surface plots of the temperature and pressure dependence of the virus particle concentration for species with (A) a low degree of dissociation, $[P_n]_L$, according to eq 16, and (C) a high degree of dissociation, $[P_n]_H$, according to eq 17. (B) and (D) show the contour plots for $[P_n]_L$ versus pressure and $[P_n]_H$ versus pressure, respectively, at distinct temperatures.

system. By using these parameters in eq 11, we obtained the analytical function for the pressure and temperature dependence of $\hat{\alpha}(P)$, and by using $C_{Pn} = 4.375 \times 10^{-6}$ mol/L in eqs 14 and 15, it was possible to calculate $[P_n]$ and $[P]$ (Figure 3A and C) and the respective surface curves and contour plots for the distinct temperature values (Figure 3B and D). Figure 3B shows that the viral particle concentration ($[P_n]$) decreased significantly with increasing pressure. This tendency was more significant at temperatures between 0 and 24 °C, while at higher temperatures (32 and 40 °C) there was less pressure-induced dissociation. The inverse relationship between temperature and viral dissociation (Figure 3C, D) was the opposite with respect to P formation. Viral dissociation became more difficult with increasing temperature.

The fraction of each species calculated from the $[P_n]$ data was used to calculate values for f_L and f_H (Figure 1D) and the viral particle concentration ($[P_n]$) at any pressure and temperature (Figure 3A). These data can be used in eqs 16 and 17 to obtain the theoretical concentrations of the associated species, $[P_n]_L$ and $[P_n]_H$, under any condition. Figure 4A, C shows the concentration of species L and H in terms of the surface response, and Figure 4B, D shows the respective diagram levels for distinct temperatures. Figure 4B indicates that an increase in temperature increased the number of viral particles with a lower tendency to dissociate (P_{nL}) and that an increase in pressure reduced this amount by converting the species with a low tendency to dissociation (P_{nL}) into species with a high tendency to dissociate (P_{nH}); associated species were also converted into dissociated subunits. These observations indicated that the increase in pressure reduced the Gibbs free energy of the transition from L to H. This in turn indicated that dissociation involved a situation in which the volume of the viral particle with a high tendency to dissociate (H species) was lower than that of the viral particle with a low tendency to dissociate (L species). Figure 4C, D shows that P_{nH} tended to dissociate more with increasing pressure to reach a maximum value followed by a decrease. The occurrence of this maximum reflected the initial conversion of P_{nL} to P_{nH} and, at higher pressure, an overall reduction of the associated form

dx.doi.org/10.1021/jp310219k | J. Phys. Chem. B 2012, 116, 14817−14828

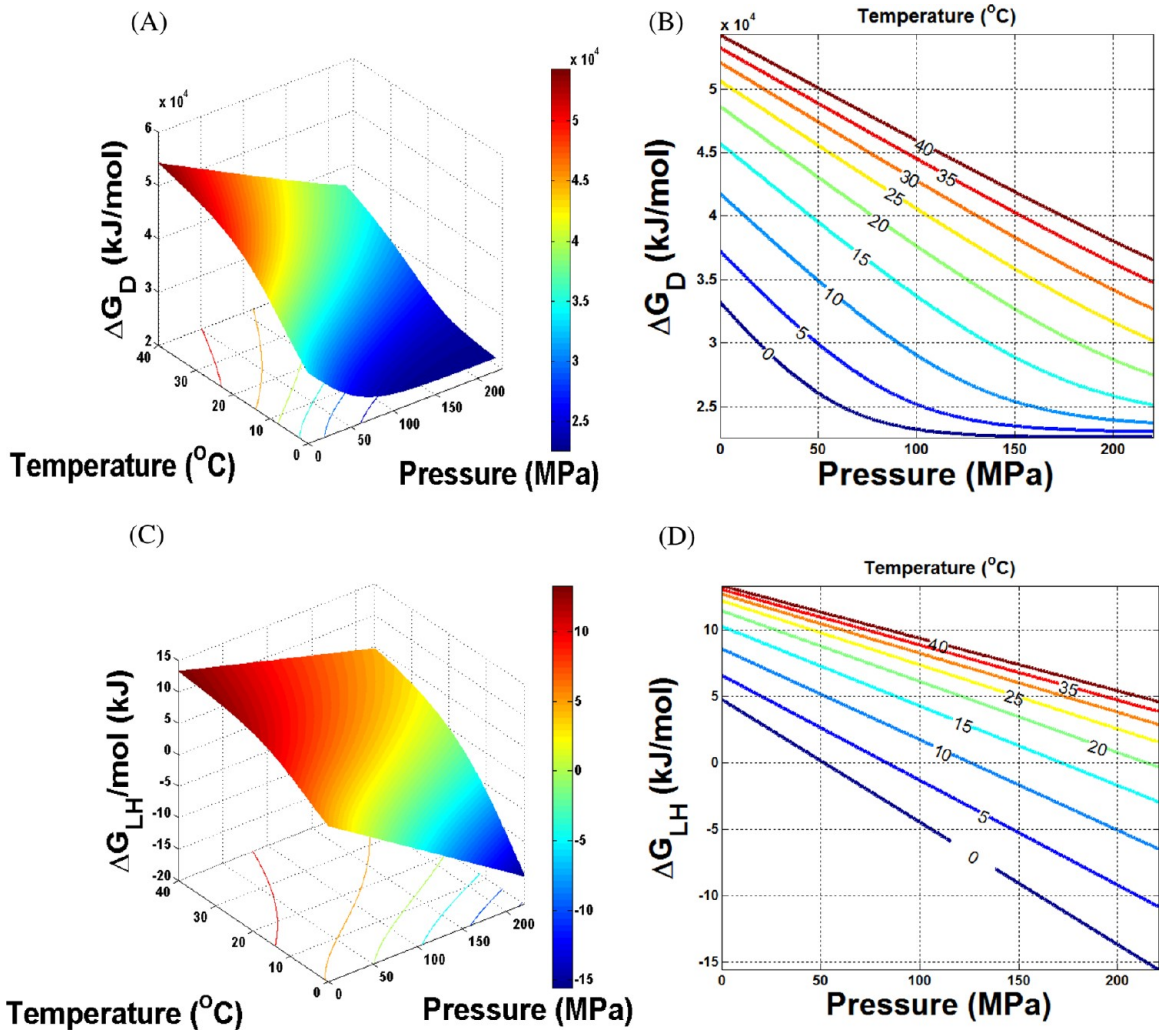

Figure 5. Surface plots of the temperature and pressure dependence of the Gibbs free energy. (A) Change in virus dissociation, ΔG_D, according to eq 19, and (C) the relationship between species with a high degree of dissociation and those with a low degree of dissociation, ΔG_{LH}, according to eq 20. (B) and (D) show the respective contour plots at different temperatures.

(P_n) (as shown in Figure 3A, B). Temperature markedly affected the maximum pressure point of $P_{n\mathrm{H}}$.

Clearly, the present approach allowed calculation of the Gibbs free energy of dissociation (ΔG_D) and transition (ΔG_{LH}) based on eqs 19 and 20, respectively. These results are shown in Figure 5A, B for the dissociation process and Figure 5C, D for the transition process. The Gibbs free energy of dissociation tended to decrease linearly with pressure at higher temperatures (Figure 5A, B). The volume change during dissociation (V_D) was calculated directly from the slopes of the curves (Figure 5B and eq 21). These values were negative, as expected for a dissociation process, and indicated that the total volume of subunit species was lower than that of the viral particle; high pressure increased the degree of dissociation of these particles. The corresponding parameters in the L−H transition were easily accessible, as shown in Figure 5C, D. The Gibbs free energy of transition decreased linearly with pressure (Figure 5D) and yielded a negative V_{LH} in which the H species had a lower volume than that the L species. The slope of the curves decreased at higher temperature, indicating a smaller change in volume. Together, these findings indicate that an increase in pressure enhanced the concentration of species $P_{n\mathrm{H}}$, $[P_n]_H$, in agreement with the results discussed above. Another point that deserves attention in this figure is that the intercept of these plots was markedly reduced at low temperature (Figure 5D).

Investigation of the volumetric properties of proteins can provide very useful insights into protein hydration and intraglobular packing.[37,38] In this work, the volume change of the dissociation profile (V_D) at different temperatures and pressures was easily assessed by using eq 21. Figure 6A shows the corresponding surface plot, the accuracy of which is directly related to the accuracy of the first and second fits used to describe the control parameters. The corresponding level diagrams are shown with respect to surface cuts at different temperatures (Figure 6B), volume changes during dissociation (Figure 6C), and pressure conditions (Figure 6D). Figure 6B shows that at ≥30 °C the pressure-induced dissociation was only slightly pressure-dependent, with volume changes ranging from −8 to about −5 mL/mol of subunit. At lower temperatures, the initial volume change during dissociation was greater; the volume change showed the greatest dependence on pressure at 0 °C, with V_D = −79 mL/mol of subunit, but decreased to close to zero at high pressures. As this plot shows, high pressure always decreased the volume change during dissociation, and high temperature reduced the dependency of V_D on pressure. Dissociation appeared to

dx.doi.org/10.1021/jp310219k | J. Phys. Chem. B 2012, 116, 14817−14828

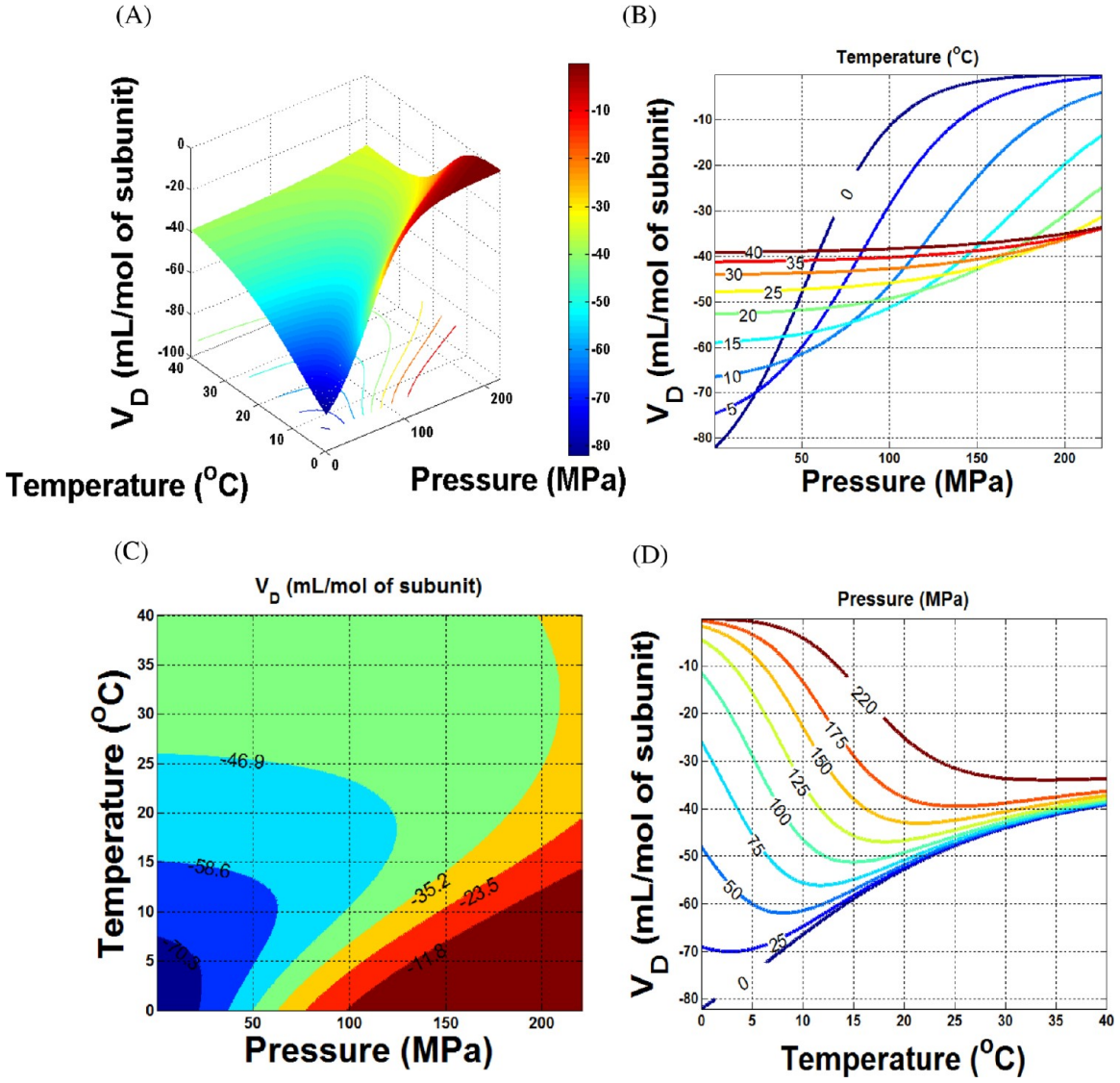

Figure 6. (A) Surface plot of the temperature and pressure dependence of volume change during dissociation, V_D, according to eq 21. (B), (C), and (D) show the contour plots of V_D versus pressure at different temperatures, temperature versus pressure at distinct V_D values, and V_D versus temperature at distinct pressure values, respectively.

decrease the volume change by partially exposing the protein−protein interface. Indeed, previous studies have shown that partial dissociation of TMV by urea[24] and by increasing the pH from 3.8 to 9.0[25] significantly decreased the absolute volume change during dissociation. Annelid extracellular hemoglobin, another protein that forms high aggregates, also showed significantly lower values of V_D during partial dissociation caused by increasing the pH of the medium.[39]

Figure 6C illustrates the usefulness of the presented approach. This figure clearly shows that the highest modulus of the volume change during dissociation occurred at low temperature and pressure. Figure 6B shows, for instance, that a V_D of approximately −49 mL/mol of subunit was reached at some combinations of temperature and pressure. This value of V_D suggests that it is possible to work at atmospheric pressure and 25 °C, and at 0 °C and a pressure of 49.9 MPa as well. The question as to which is the "least expensive" and most efficient option for a given process, i.e., one that works at 24 °C or at 0 °C and 49.9 MPa, can be answered by consulting Figure 6D. This figure shows that at a moderate pressure of 63.4 MPa there is a point of inflection close to 10 °C at which the modulus for volume change during dissociation is maximal and equal to V_D = −59.5 mL/mol of subunit. This temperature represents the point of optimum operation at this pressure since the modulus for volume change during dissociation is maximal, thereby facilitating virus dissociation. As the pressure increases, the curve changes from hyperbolic at 0.55 MPa to sigmoid at 220.6 MPa and passes through an inflection point that gradually disappears at increasing pressures (Figure 6D).

Another important point involves the maximization of entropy, a condition that partly facilitates dissociating by contributing to a lower Gibbs free energy. As shown here, it was possible to describe the behavior of entropy as the change in $-T\Delta S_D$ during TMV dissociation (eq 22) at different temperatures and pressures (Figure 7A). The level diagram shows the surface cuts at different temperatures (Figure 7B). As expected, the change in entropy during dissociation was negative at most of the temperatures and pressures; i.e., the entropy of the virus subunit was lower than that of the virus particle. At low temperature, there was an increase in the

dx.doi.org/10.1021/jp310219k | J. Phys. Chem. B 2012, 116, 14817−14828

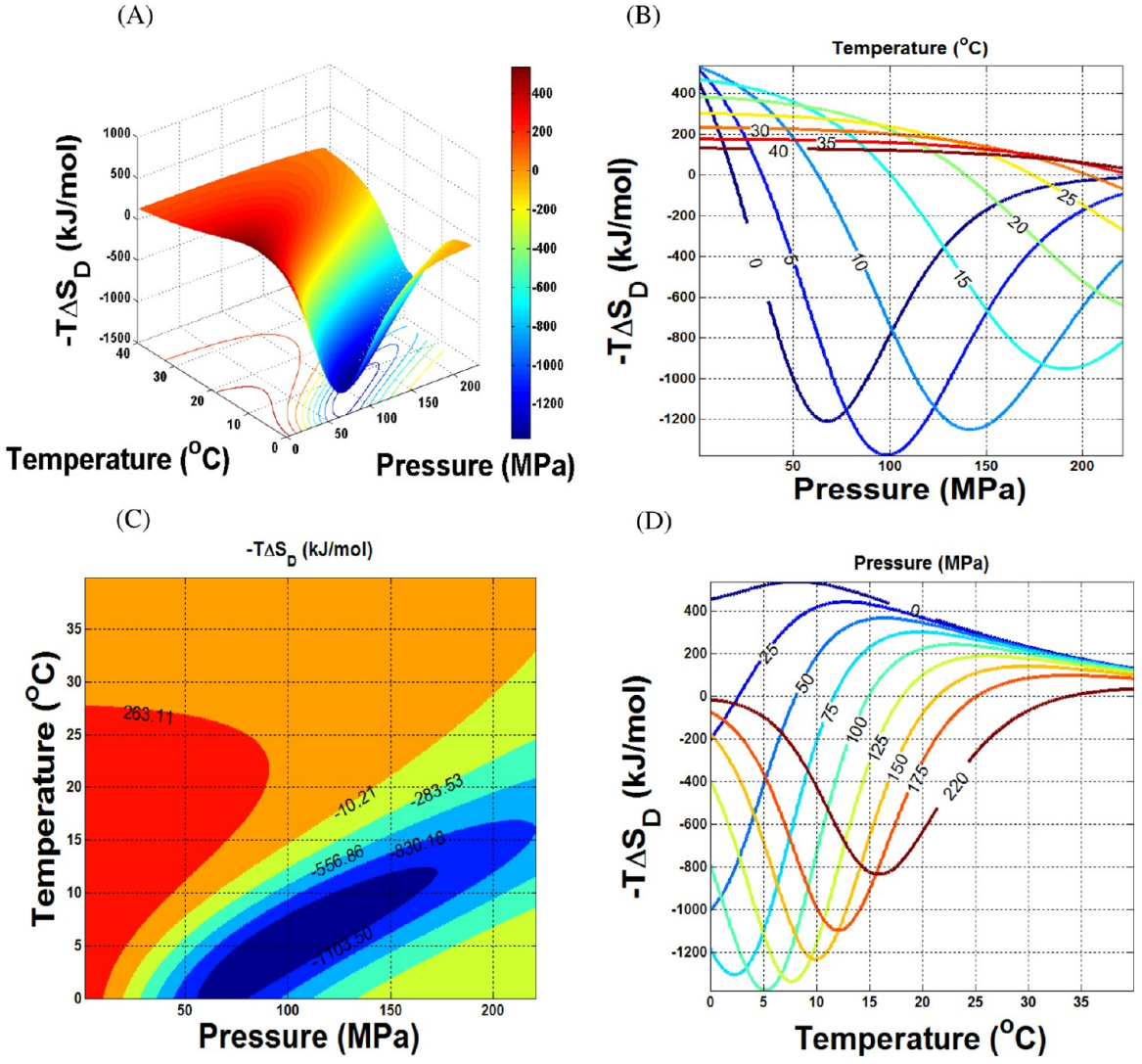

Figure 7. (A) Surface plot of the temperature and pressure dependence of the change in negative entropy during dissociation, $T\Delta S_D$, according to eq 22, and the respective contour plots of $T\Delta S_D$ versus pressure (B) and versus temperature values (D). (C) Two-dimensional contour graph of $-T\Delta S_D$ as a function of temperature and pressure.

modulus of the change in entropy followed by a significant decrease with increasing pressure; this phenomenon was not observed at high temperatures. Entropy increased within a small range of temperature and pressure (from close to zero to 10 °C and at 50−160 MPa; Figure 7B, C).

Figure 8 shows the change in enthalpy during dissociation. The overall profile was less complex than for entropy. Enthalpy was higher at higher temperatures and lower pressures. Interestingly, dissociation was an enthalpy-driven process at all pressures and temperatures since the values were all higher than $T\Delta S$ (Figures 7 and 8). Stites[40] mentioned that numerous studies had found dissociation to be an entropy-driven process. Although enthalpy predominated in the dissociation studied here, this characteristic was not necessarily uniform since it depended on the experimental conditions to which the protein was exposed, with possible switching from an enthalpy- to an entropy-driven process.

The thermodynamics of TMV dissociation studied here are very relevant physiologically since virus association and dissociation are important steps in the process of infection. Moreover, the temperatures to which a plant is subjected may interfere directly with the viral cycle in the plant cell. Overall, the use of extent of reactions can be helpful in analyzing biochemical processes in several systems and in identifying variables that can serve as predictors. This approach can be applied to several other systems that involve physical and chemical processes.

CONCLUSIONS

The most important aspect of this work was a description of the temperature and pressure dependence of the volume and entropy of virus dissociation. The presented approach provides a powerful means of easily characterizing this system. The procedure can also be applied with high precision to other processes such as protein aggregation, bacterial growth, enzyme kinetics, and fermentation. In these cases, the only modification needed is the way in which the parameters related to concentrations and velocities of reaction are calculated. In addition, despite the fact that we considered only two states or degrees of dissociation associated with two species in solution (one with a high degree of dissociation, H, and the other with a low degree of dissociation, L), a third state could be easily introduced into eq 10 to provide more precise adjustment in

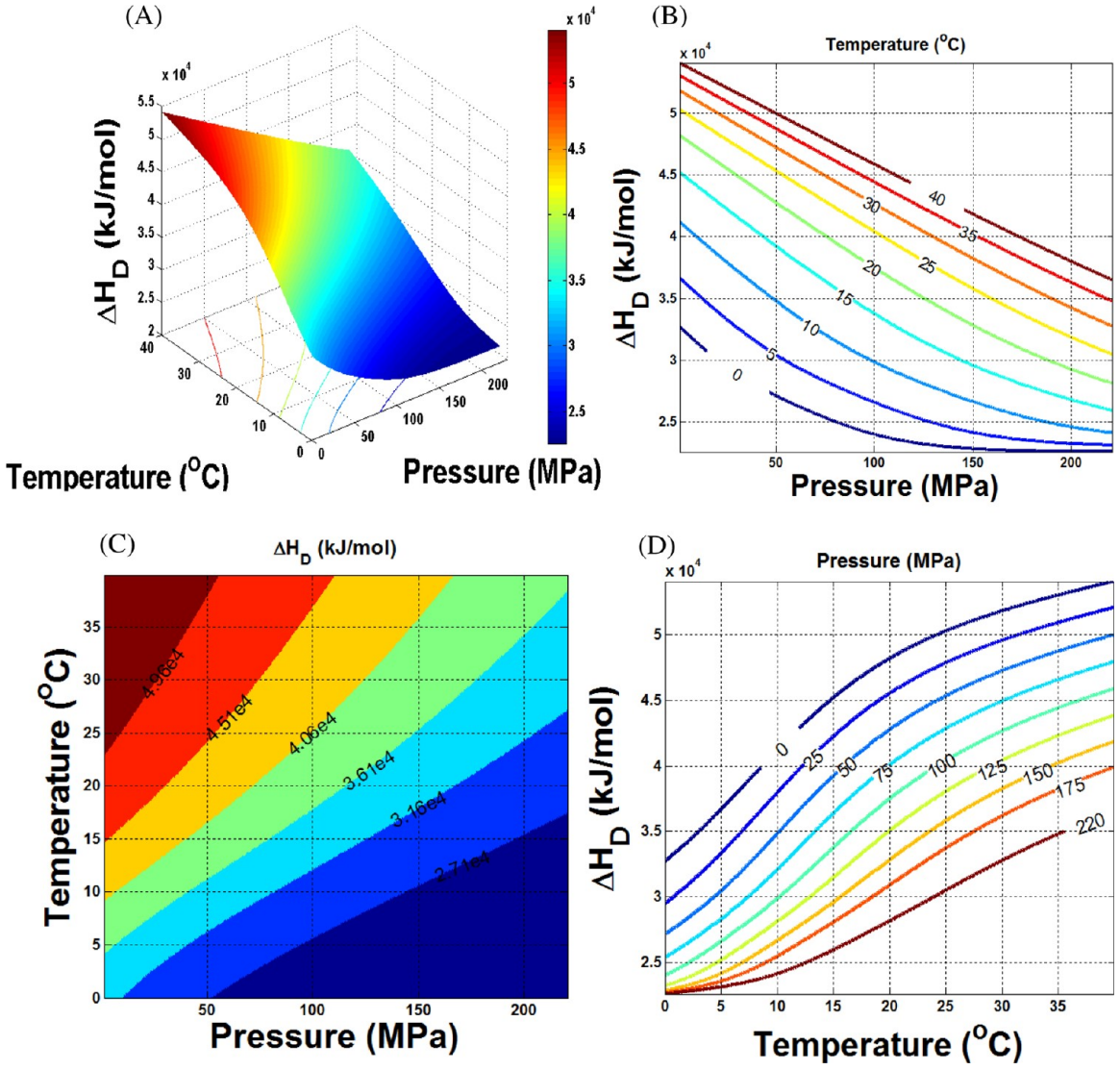

Figure 8. (A) Surface plot of the temperature and pressure dependence of the change in enthalpy during dissociation, ΔH_D, according to eq 23, and the respective contour plots of ΔH_D versus pressure (B) and ΔH_D versus temperature (D). (C) Two-dimensional contour graph of ΔH_D as a function of temperature and pressure.

more complex situations. Another important aspect of this procedure is its ability to predict intermediate values between two points of experimental data, as well as extreme values above or below the range of experimental data. The approach described here should be useful in thermodynamic analyses of complex molecular phenomena.

AUTHOR INFORMATION

Corresponding Author

*Fax +55-75-3161-8056; phone +55-75-3161-8055; e-mail jose.a.c.bispo@gmail.com.

Notes

The authors declare no competing financial interest.

ACKNOWLEDGMENTS

The authors thank Stephen Hyslop for editing the English of the manuscript. This work was supported by Fundação de Amparo à Pesquisa do Estado da Bahia (FAPESB), Fundação de Amparo à Pesquisa do Estado de São Paulo (FAPESP), Conselho Nacional de Desenvolvimento Científico e Tecnológico (CNPq), and Coordenação de Aperfeiçoamento de Pessoal de Nível Superior (CAPES), Brazil.

DEFINITIONS OF NOTATIONS

f_H, f_L	Fraction of the species H and L
k	Molar compressibility coefficient (for forms H and L, k_L and k_H, and $k_1 = k_H - k_L$)
K_D	Equilibrium constant of dissociation
n	Number of subunits
P_n	Viral particles (for high and low tendency to dissociate, P_{nH} and P_{nL})
I	Light scattering intensity of TMV
u	Independent property
V_D	Volume change of dissociation
w	Fitting parameter of the natural logarithm of the initial virus concentration (for forms H and L, w_H and w_L, and $w_1 = w_L - w_H$)
x	Extent of reaction
α_i	Degree of dissociation of species i
$\hat{\alpha}$	Average degree of dissociation ($\equiv \alpha_D$)

dx.doi.org/10.1021/jp310219k | J. Phys. Chem. B 2012, 116, 14817−14828

ΔG_D, ΔG_{LH}	Gibbs free energy of dissociation and of transition from L to H
ΔH_D	Enthalpy of dissociation
ΔS_D	Entropy of dissociation
θ_M	Molar thermal expansibility coefficient
v	Velocity of reaction

REFERENCES

(1) Silva, J. L.; Miles, E. W.; Weber, G. *Biochemistry* **1986**, *25*, 5780−5786.
(2) Silva, J. L.; Foguel, D.; Da Poian, A. T.; Prevelige, P. E. *Curr. Opin. Struct. Biol.* **1996**, *6*, 166−175.
(3) Weber, G.; Drickamer, H. G. *Q. Rev. Biophys.* **1983**, *16*, 89−112.
(4) Ishimaru, D.; Sá-Carvalho, D.; Silva, J. L. *Vaccine* **2004**, *22*, 2334−2339.
(5) Tian, S. M.; Ruan, K. C.; Qian, J. F.; Shao, G. Q.; Balny, C. *Eur. J. Biochem.* **2000**, *267*, 4486−4494.
(6) Gaspar, L. P.; Mendes, Y. S.; Yamamura, A. M. Y.; Almeida, L. F. C.; Caride, E.; Goncalves, R. B.; Silva, J. L.; Oliveira, A. C.; Galler, R.; Freire, M. S. *J. Virol. Methods* **2008**, *150*, 57−62.
(7) Oliveira, A. C.; Ishimaru, D.; Goncalves, R. B.; Smith, T. J.; Mason, P.; Sá-Carvalho, D.; Silva, J. L. *Biophys. J.* **1999**, *76*, 1270−1279.
(8) Kingsley, D. H.; Hollinian, D. R.; Calci, K. R.; Chen, H. Q.; Flick, G. J. *Appl. Environ. Microbiol.* **2007**, *73*, 581−585.
(9) Bradley, D. W.; Hess, R. A.; Tao, F.; Sciaba-Lentz, L.; Remaley, A. T.; Laugharn, J. A.; Manak, M. *Transfusion (Paris)* **2000**, *40*, 193−200.
(10) Gaspar, L. P.; Johnson, J. E.; Silva, J. L.; Da Poian, A. T. *J. Mol. Biol.* **1997**, *273*, 456−466.
(11) Da Poian, A. T.; Oliveira, A. C.; Gaspar, L. P.; Silva, J. L.; Weber, G. *J. Mol. Biol.* **1993**, *231*, 999−1008.
(12) Pontes, L.; Cordeiro, Y.; Giongo, V.; Villas-Boas, M.; Barreto, A.; Araujo, J. R.; Silva, J. L. *J. Mol. Biol.* **2001**, *307*, 1171−1179.
(13) Silva, J. L.; Oliveira, A. C.; Gomes, A. M. O.; Lima, L. M. T. R.; Mohana-Borges, R.; Pacheco, A. B. F.; Foguel, D. *Biochim. Biophys. Acta, Protein Struct. M* **2002**, *1595*, 250−265.
(14) Bonafe, C. F. S.; Glaser, M.; Voss, E. W.; Weber, G.; Silva, J. L. *Biochem. Biophys. Res. Commun.* **2000**, *275*, 955−961.
(15) Jurkiewicz, E.; Villas-Boas, M.; Silva, J. L.; Weber, G.; Hunsmann, G.; Clegg, R. M. *Proc. Natl. Acad. Sci. U.S.A.* **1995**, *92*, 6935−6937.
(16) Norberto, D. R.; Vieira, J. M.; Souza, A. R.; Bispo, J. A. C.; Bonafe, C. F. S. *Open J. Biophys.* **2012**, *2*, 4−14.
(17) Santos, J. L. R.; Aparicio, R.; Joekes, I.; Silva, J. L.; Bispo, J. A. C.; Bonafe, C. F. S. *Biophys. Chem.* **2008**, *134*, 214−224.
(18) Culver, J. N. *Annu. Rev. Phytopathol.* **2002**, *40*, 287−308.
(19) Pallas, V.; Garcia, J. A. *J. Gen. Virol.* **2011**, *92*, 2691−2705.
(20) Klug, A. *Philos. Trans. R. Soc., B* **1999**, *354*, 531−535.
(21) Namba, K.; Pattanayek, R.; Stubbs, G. *J. Mol. Biol.* **1989**, *208*, 307−325.
(22) Abel, P. P.; Nelson, R. S.; De, B.; Hoffmann, N.; Rogers, S. G.; Fraley, R. T.; Beachy, R. N. *Science* **1986**, *232*, 738−743.
(23) Wu, X. J.; Beachy, R. N.; Wilson, T. M.; Shaw, J. G. *Virology* **1990**, *179*, 893−895.
(24) Bonafe, C. F. S.; Vital, C. M. R.; Telles, R. C. B.; Goncalves, M. C.; Matsuura, M. S. A.; Pessine, F. B. T.; Freitas, D. R. C.; Vega, J. *Biochemistry* **1998**, *37*, 11097−11105.
(25) Santos, J. L. R.; Bispo, J. A. C.; Landini, G. F.; Bonafe, C. F. S. *Biophys. Chem.* **2004**, *111*, 53−61.
(26) Silva, J. L.; Villas-Boas, M.; Bonafe, C. F. S.; Meirelles, N. C. *J. Biol. Chem.* **1989**, *264*, 15863−15868.
(27) Bonafe, C. F. S.; Villas-Boas, M.; Suarez, M. C.; Silva, J. L. *J. Biol. Chem.* **1991**, *266*, 13210−13216.
(28) Bonafe, C. F. S.; Araujo, J. R. V.; Silva, J. L. *Biochemistry* **1994**, *33*, 2651−2660.
(29) Orlov, V. N.; Arutyunyan, A. M.; Kust, S. V.; Litmanovich, E. A.; Drachev, V. A.; Dobrov, E. N. *Biochemistry (Moscow)* **2001**, *66*, 154−162.
(30) Rafikova, E. R.; Kurganov, B. I.; Arutyunyan, A. M.; Kust, S. V.; Drachev, V. A.; Dobrov, E. N. *Int. J. Biochem. Cell Biol.* **2003**, *35*, 1452−1460.
(31) Asselin, A.; Zaitlin, M. *Virology* **1978**, *91*, 173−181.
(32) Paladini, A. A.; Weber, G. *Rev. Sci. Instrum.* **1981**, *52*, 419−427.
(33) Tanford, C. *Physical chemistry of macromolecules*; Wiley: New York, 1961.
(34) Bispo, J. A. C.; Bonafe, C. F. S.; de Souza, V. B.; Silva, J. B. A.; Carvalho, G. B. M. *J. Math. Chem.* **2011**, *49*, 1976−1995.
(35) Bispo, J. A. C.; Bonafe, C. F. S.; Koblitz, M. G. B.; Silva, C. G. S.; Souza, A. R. *J. Math. Chem.* **2012**, in press.
(36) Baini, R.; Langrish, T. A. G. *J. Food Eng.* **2007**, *79*, 330−343.
(37) Silva, J. L.; Weber, G. *Annu. Rev. Phys. Chem.* **1993**, *44*, 89−113.
(38) Chalikian, T. V. *Annu. Rev. Biophys. Biomol. Struct.* **2003**, *32*, 207−235.
(39) Bispo, J. A. C.; Santos, J. L. R.; Landini, G. F.; Goncalves, J. M.; Bonafe, C. F. S. *Biophys. Chem.* **2007**, *125*, 341−349.
(40) Stites, W. E. *Chem. Rev.* **1997**, *97*, 1233−1250.